Carbon 243 (2025) 120508

Contents lists available at ScienceDirect

Carbon

journal homepage: www.elsevier.com/locate/carbon

Metal phthalocyanines and imidazolium bromide Copolymers supported on multi-walled carbon nanotubes: a "lego-like" assembly of hybrid bifunctional materials applied for CO_2 conversion

Benedetto Taormina [a,b], Rémy Jouclas [b], Alwyn Dsouza [b], Anthony Morena [b], Michelangelo Gruttadauria [a], Carmela Aprile [b,*], Francesco Giacalone [a]

[a] Department of Biological, Chemical and Pharmaceutical Sciences and Technologies, University of Palermo and INSTM UdR Palermo, Viale delle Scienze, Ed. 17 90128, Palermo, Italy
[b] UCNANO, Department of Chemistry, CMA Lab., NISM, University of Namur, Belgium, 61 rue de Bruxelles, 5000, Namur, Belgium

ARTICLE INFO

Keywords:
Metal-phthalocyanine
CO_2 valorization
Cyclic carbonates
Carbon nanotubes
Bifunctional catalyst
Hybrid materials

ABSTRACT

The present study explores the development of hybrid heterogeneous bifunctional catalysts supported on multi-walled carbon nanotubes (MWCNT) for CO_2 valorization in the synthesis of cyclic carbonates. These materials integrate both nucleophilic species (imidazolium bromide) and Lewis acid species (magnesium, copper, and zinc phthalocyanines), revealing improved catalytic activity through synergistic effects. MWCNT are employed as support enhancing the accessibility of active sites and the overall catalytic performance. Three different metal-phthalocyanines with imidazole moieties (**MgPC-Im$_4$**, **CuPC-Im$_4$** and **ZnPC-Im$_4$**) were covalently anchored onto MWCNT through an atom economic polymerization process, resulting in new bifunctional materials (**MPC@MWCNT**) in which the polymeric network fully covers the nanotubes longitudinally. Comprehensive characterization of the hybrids by using different techniques confirmed the successful synthesis of these materials. Catalytic testing of the **MPC@MWCNT** materials in epoxide-CO_2 cycloaddition reactions revealed that the **MgPC@MWCNT** hybrid exhibited superior catalytic activity compared to its unsupported counterpart, highlighting the benefits of the MWCNT as support (TON = 8050 *vs* TON = 7120), reaching very high TON values (up to 19920) at very low catalytic loadings (0.004–0.0013 mol% based on metal content). Importantly, this study introduces a simple yet effective novel method for covalently attaching high amounts of metal-phthalocyanines onto MWCNT. Potentially, the "lego-like" approach of this method allows for the creation of diverse materials with different metal centres, enabling access to a number of different applications in the field of Materials Science.

1. Introduction

The sharp rise in CO_2 emissions, primarily from fossil fuel combustion, has intensified environmental concerns, highlighting the urgent need for efficient solutions [1,2]. Green chemistry principles [3], particularly catalysis, atom economy, and use of renewable feedstocks, provide essential guidance, emphasizing the need to design both chemical processes and systems that minimize environmental impact and significantly reduces energy consumption. Carbon capture, utilization and storage approaches represent a series of promising technologies gaining increasing attention. In particular, conversion of CO_2 into value added chemicals constitutes an efficient solution, which not only could contribute to atmospheric CO_2 reduction, but also may converts it into valuable products [4,5]. One example of such approach consists in the cycloaddition of CO_2 with epoxides to produce cyclic carbonates [6,7], versatile compounds used as chemical intermediates, solvents, and battery electrolytes [8–10]. However, any transformation of CO_2 remains energy demanding due to its thermodynamic stability ($\Delta G_0 = -394$ kJ mol^{-1}). Alternatively, catalytic species can be employed to bypass this barrier, enabling more efficient processes. In line with the afore-mentioned green principles, employing a catalyst is the optimal approach for CO_2 transformation, particularly if a heterogeneous catalyst is considered: indeed, heterogeneous catalysts facilitate the recovery and recycling over homogeneous ones, enhancing the overall efficiency

* Corresponding author.
E-mail addresses: carmela.aprile@unamur.be (C. Aprile), francesco.giacalone@unipa.it (F. Giacalone).

https://doi.org/10.1016/j.carbon.2025.120508
Received 9 April 2025; Received in revised form 22 May 2025; Accepted 2 June 2025
Available online 5 June 2025
0008-6223/© 2025 The Authors. Published by Elsevier Ltd. This is an open access article under the CC BY license (http://creativecommons.org/licenses/by/4.0/).

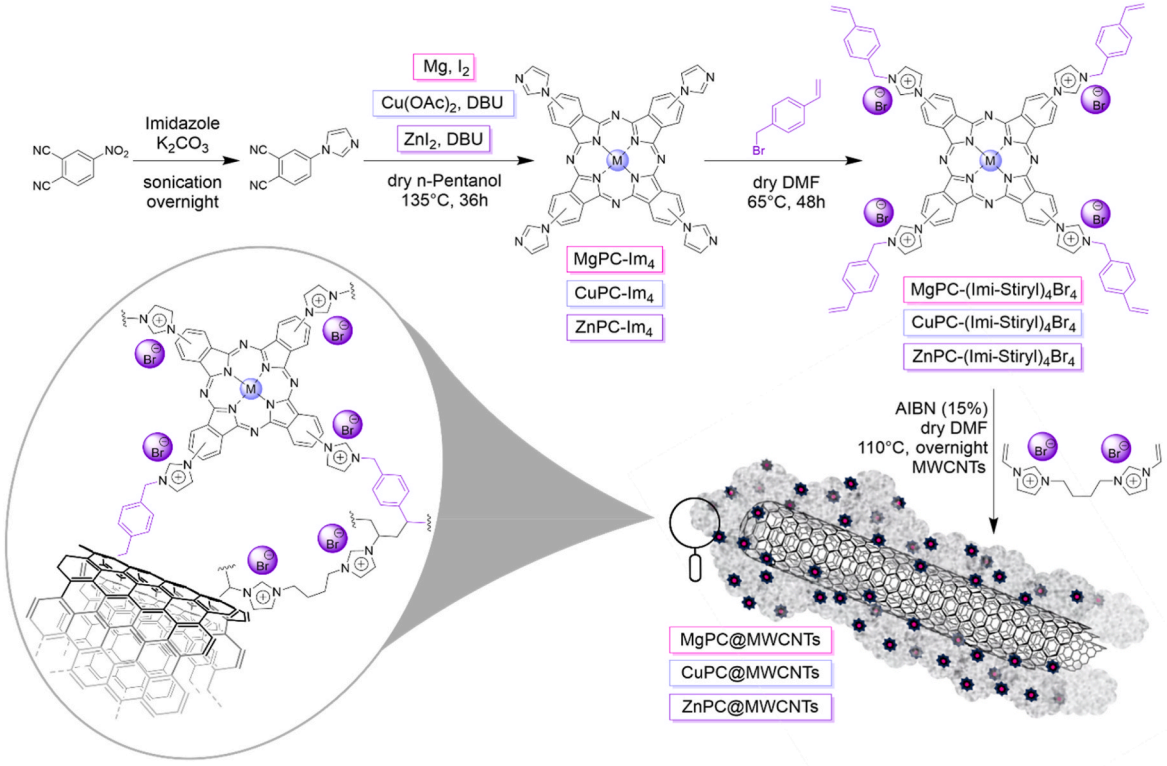

Fig. 1. Synthetic procedure for the preparation of the various **MPC@MWCNT**.

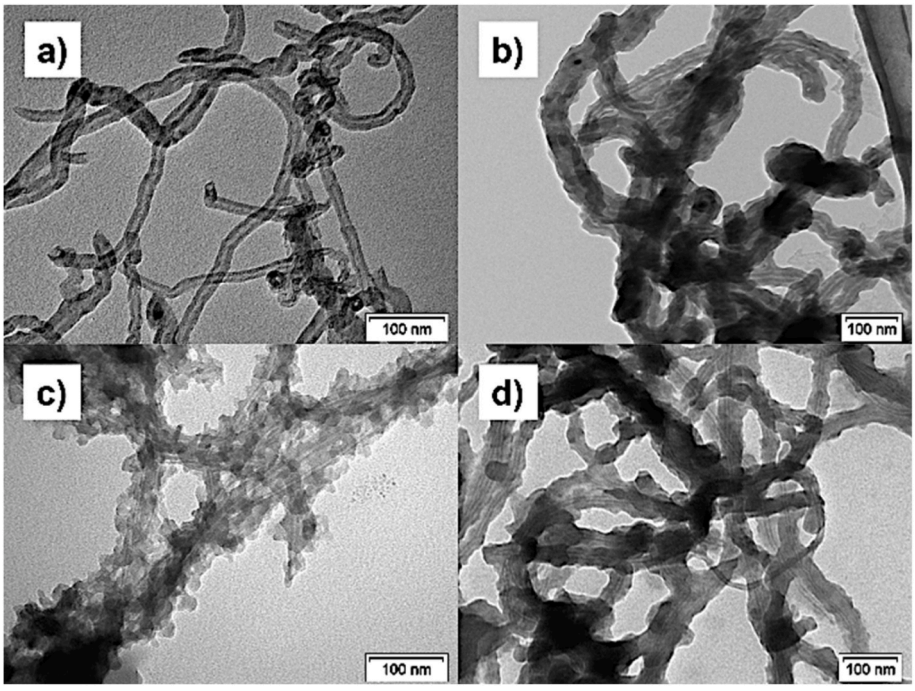

Fig. 2. TEM micrographs of a) pristine **MWCNT**; b) **MgPC@MWCNT**; c) **CuPC@MWCNT**; d) **ZnPC@MWCNT**.

and sustainability of the process [11–17]. During these last years, it was reported that the activity of a catalytic system is greatly enhanced by the synergistic combined action of a nucleophile (chloride, bromide, iodide anions, etc.) which facilitates the opening of the epoxydic ring, and a Lewis acid metal centre (magnesium, aluminium, nickel (II), copper (II), zinc (II), etc.) that can coordinate the electron-rich species involved in the reaction. Notably, it has been observed that such effect is enhanced when the nucleophilic catalyst and the Lewis acid co-catalyst are in close proximity. Thus, a practical and sustainable alternative involves the use of heterogeneous bifunctional catalysts, which integrate both the metal cation and nucleophilic species within a single material [18–23]. In our previous work [23], we reported the utilization of two cross-linked heterogeneous bifunctional materials (**MgPC-BIBI-Br** and **MgPC–SI-BI–Br**) that incorporate magnesium phthalocyanine (**MgPC**) and

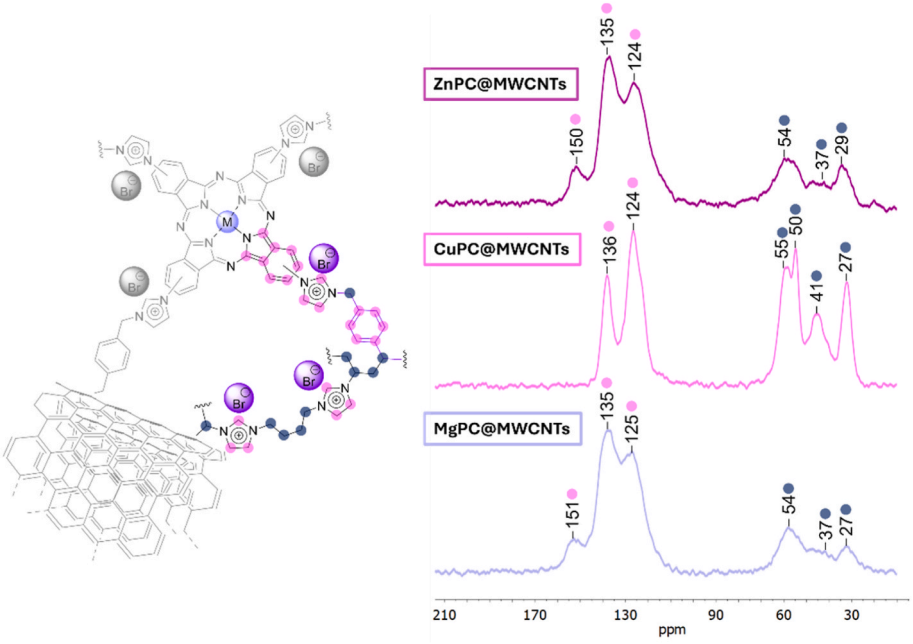

Fig. 3. Solid state CP-TOSS-MAS ^{13}C NMR spectra of **MgPC@MWCNT**, **CuPC@MWCNT** and **ZnPC@MWCNT**,

imidazolium bromide (**ImiBr)** moieties as catalysts for the synthesis of cyclic carbonates through the cycloaddition of epoxides with CO_2, gaining excellent results. In the present work, instead, maintaining the green and sustainable attitude outlined earlier, the objective was to develop materials supported on multi-walled carbon nanotubes (MWCNT) to observe their characteristics and catalytic performances. Alongside other carbon nanoforms, MWCNT exhibit excellent thermal stability, remarkable mechanical strength, and a large functionalizable surface area, making them highly suitable scaffolds for the development of heterogeneous materials [24–26]. In addition to that, in previous studies, it has been demonstrated that, depending on the polymerization technique, MWCNT can effectively influence the polymer growth process, ultimately resulting in a uniform polymer coating around the carbonaceous scaffold [27–30]. The hypothesis is that this approach will provide a material in which the accessibility of active sites is enhanced compared to the one of catalysts discussed in the previous work [23]. Consequently, this increased accessibility is expected to improve catalytic activity, thereby offering valuable insights into the differences between supported and non-supported systems. For this case of study, three different metal-phthalocyanines tetrasubstituted with imidazole moieties (**MPC-Im$_4$**, i.e. **MgPC-Im$_4$**, **CuPC-Im$_4$** and **ZnPC-Im$_4$**) have been covalently attached onto MWCNT in large amount together with imidazolium bromide moieties. This combination resulted in a new set of heterogeneous bifunctional materials (**MPC@MWCNT**) that, after having undergone a comprehensive characterization, have successfully been tested as catalyst in the cycloaddition of epoxides and CO_2 to give cyclic carbonates, reaching good levels of conversion and excellent levels of selectivity. In the past years, ionic liquids have been used as solvent for various processes mediated by metal–phthalocyanines [31, 32]. Nevertheless, in the literature there are just few examples where both ionic liquids and metal–phthalocyanines are used in combination for specific purposes [33–35], and even fewer where this combination is applied to the synthesis of cyclic carbonates [23,36]. Notably, to the best of our knowledge, no studies have yet described MWCNT-supported bifunctional heterogeneous materials based on imidazolium bromide and metal-phthalocyanines applied for the thermo-induced conversion of CO_2 into cyclic carbonates in the presence of epoxides. Additionally, this work presents a simple and effective method for easily attaching large amounts of metal phthalocyanines to MWCNT through an atom-economic strategy, with flexibility in metal selection.

2. Materials and methods

Chemicals and solvents were sourced from commercial suppliers and utilized without additional purification. MWCNT (OD: 10–20 nm; L: 1–2 μm; Lot:TCP004003) were provided by IOLITEC. AIBN stands for "Azobisisobutyronitrile. The synthesis procedures for several compounds, including **MgPC-Im$_4$**, **MgPC-(Imi-Styryl)$_4$Br$_4$**, **Bis-Vinyl-Imi-Br**, and 1-(bromomethyl)-4-vinylbenzene have been previously documented in earlier research [23]. IR spectra have been recorded on an Agilent Technologies Cary 630 Fourier Transform-Infrared (FT-IR) spectrometer, with an attenuated total reflectance (ATR) technology. For imaging, Transmission Electron Microscopy (TEM) was conducted using a Philips Tecnai 10 microscope operating at 80 kV. Sample preparation involved dispersing a small amount of material in absolute ethanol, which was then deposited onto a copper grid. X-ray Photoelectron Spectroscopy (XPS) analyses were performed with a Thermo Fisher ESCALAB 250Xi instrument, equipped with a monochromatic Al Kα X-ray source (1486.6 eV) and a hemispherical deflector analyzer (SDA) set to a constant pass energy (CAE). A 200 μm diameter X-ray spot was utilized for the experiments. To mitigate sample charging, a flood gun providing low-energy electrons and argon ions was employed. The analysis chamber was maintained at an approximate pressure of 10^{-8} Torr during data collection. Survey spectra were recorded at a pass energy of 200 eV, while high-resolution spectra were collected at a pass energy of 20 eV. For the XPS analysis of the precursors and the materials presented in this study, data were collected from five different surface points on each sample. Numerical values eventually associated to this analysis presented here are the averages of the measurements obtained from these five points for each sample. Peak analysis was conducted using Thermo Avantage software, employing a non-linear least squares fitting approach that incorporated a weighted sum of Lorentzian and Gaussian components. Background subtraction followed the Shirley and Sherwood methods. Thermogravimetric analysis (TGA) was carried out under N_2 flow or air flow, covering a temperature range from 25 to 900 °C with a heating rate of 10 °C/min, using a Mettler Toledo TGA STAR system An isotherm ramp of 30 min at 100 °C was employed to equilibrate the sample analysis after the loss of water naturally adsorbed onto the samples. To avoid displaying weight losses associated with water evaporation, TGA data presented here begin at 100 °C. Chemical combustion analysis was performed using a Flash 1112 series EA

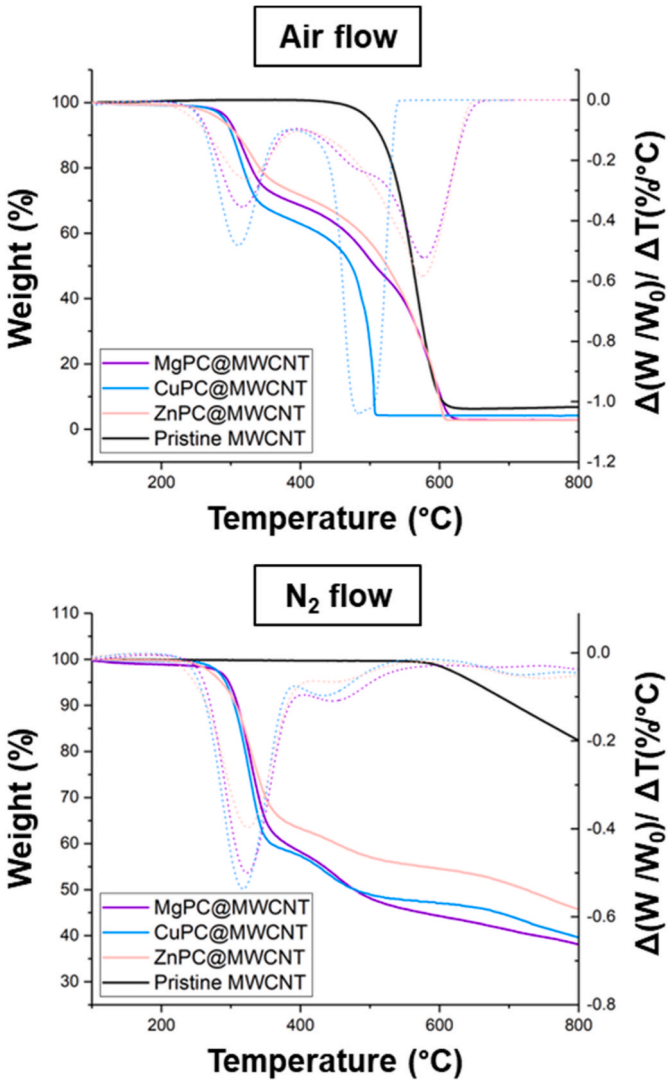

Fig. 4. TGA (solid lines) and DTG (dotted lines) under Air flow (up) and N_2 flow (down) of **MgPC@MWCNT**, **CuPC@MWCNT** and **ZnPC@MWCNT**. In all graphics black lines refer to pristine **MWCNT**.

ThermoFischer – Interscience with a GC-TCD detector. CHNS analysis operates in two steps: 1. An oxidation-reduction reactor (containing Cu) is placed in a furnace at 950 °C under a continuous helium flow. The precisely weighed sample is introduced into the reactor, followed by a brief injection of oxygen to initiate the oxidation or reduction reaction, depending on the sample. This process generates various gases: carbon produces CO_2, hydrogen forms H_2O, nitrogen generates N_2, and sulfur produces SO_2. 2. These gases are then separated in a gas chromatography (GC) column, and their concentrations are determined based on their intensity and a calibration curve. Using the precisely measured sample mass, the concentration values allow us to calculate the percentage of each element in the sample. Nitrogen adsorption-desorption measurements were performed at −196.15 °C using a volumetric adsorption analyzer (Micromeritics ASAP 2420). Before the analysis, the samples underwent pre-treatment at 150 °C for 8 h under vacuum conditions (0.1 mbar). For nuclear magnetic resonance (NMR) spectroscopy, ^{1}H liquid-state spectra were recorded at room temperature on a JEOL ECX 500 MHz spectrometer operating at 9.4 T, equipped with a broadband 5 mm probe with a pulse of 45° and a recycle delay 6.6s. Solid-state nuclear magnetic resonance Magic Angle Spinning (MAS) ^{13}C spectra were recorded at room temperature, on a Jeol ECZ-R 600 MHz spectrometer operating at 14.1 T, using 3.2 mm zirconia rotors, a spinning rate of 10 kHz and an automas probe. Total suppression of spinning sidebands (TOSS) cross-polarization (CP) experiments on ^{13}Cwere carried out using a relaxation delay of 5 s, acquisition time of 18 ms, and SPINAL64 proton decoupling using a contact time of 2 ms. TOSS timing was fixed to a value of 10. The total number of scans was 3103. ^{13}C Chemical shifts were referenced externally to Sodium adamantane (0 ppm).

2.1. Synthesis of CuPC-Im$_4$

4-(1*H*-imidazole-1-yl)phthalonitrile (1.50 g, 7.72 mmol, 1 eq) and $Cu(OAc)_2$ (701 mg, 3.86 mmol, 0.5 eq) were suspended in anhydrous *n*-pentanol (15 mL) under argon atmosphere in a flame-dried 100 mL test tube, then 1,8-diazabicyclo[5.4.0]undec-7-ene (DBU) (173 μL, 1.16 mmol, 15 mol%) was added to the mixture that was stirred at 135 °C for 36 h. Then the mixture was cooled to room temperature, diluted with *n*-pentanol (100 mL), sonicated for 30 min and filtered on a Millipore filtration system. The resulting precipitate was suspended in water (100 mL), stirred overnight at room temperature, then filtered and the residue was purified by subsequent soxhlet washings with pyridine and ethanol. Finally, the solid was sonicated in acetone (100 mL) for 30 min, filtered and dried under vacuum to afford 759 mg (yield 48 %) of copper tetra (imidazole-1-yl)phthalocyanine **CuPcIm$_4$** (mixture of isomers) as a dark blue powder (See Table S1-Figs. S1–S2 for additional information).

2.2. Synthesis of ZnPC-Im$_4$

4-(1*H*-imidazole-1-yl)phthalonitrile (2.00 g, 10.3 mmol, 1 eq) and ZnI_2 (1.64 g, 5.15 mmol, 0.5 eq) were suspended in anhydrous *n*-pentanol (15 mL) under argon atmosphere in a flame-dried 100 mL test tube, then DBU (231 μL, 1.55 mmol, 15 mol%) was added to the mixture that was stirred at 135 °C for 36 h. Subsequently the mixture was cooled to room temperature, diluted with *n*-pentanol (100 mL), sonicated for 30 min and filtered on Millipore. The resulting precipitate was suspended in water (100 mL), stirred overnight at room temperature, then filtered and the residue was washed *via* subsequent soxhlet with ethanol and then pyridine. The resulting pyridine filtrate was concentrated under vacuum and the residue was sonicated in DMF for 30 min, filtered and sonicated again in acetone for 30 min, filtered and dried under vacuum to afford 1.26 g (yield 58 %) of zinc tetra(imidazole-1-yl) phthalocyanine **ZnPcIm$_4$** (mixture of isomers) as a green powder (See Table S1-Figs. S1–S2 for additional information).

2.3. Synthesis of MPC-(Imi-Styryl)$_4$Br$_4$

MPC-Im$_4$ (200 mg, 0.25 mmol for **MgPC-Im4**, 0.24 mmol for **CuPC-Im4**, 0.24 mmol for **ZnPC-Im4**, 1 eq.) and 4-vinylbenzyl bromide (5 eq) were added together in a 50 mL round bottom flask under argon atmosphere, and then solubilized in 5 mL of anhydrous DMF. The resulting reaction mixture was left to stir two days at 70 °C. Subsequently, the solution was cool down to room temperature, diluted with 10 mL of acetone and then filtered to collect a precipitate which has been washed five times with 30 mL of acetone. After drying at 60 °C for 8 h, 380 mg (yield 96 %) of **MgPC-(Imi-Styryl)$_4$Br$_4$**, 370 mg (yield = 95 %) of **CuPC-(Imi-Styryl)$_4$Br$_4$** and 250 mg (yield 64 %) of **ZnPC-(Imi-Styryl)$_4$Br$_4$** (See Figs. S1–S3 for additional information)

2.4. Synthesis of MPC@MWCNT

The solid powders of **MPC-(Imi-Styryl)$_4$Br$_4$** (1 eq) and **Bis-Vinyl-Imi-Br** (4.4 eq) were finely ground using a mortar and pestle until a homogeneous mixture was achieved. MWCNT (100 mg per 0.2 mmol of **MPC-(Imi-Styryl)$_4$Br$_4$**) were then incorporated and mixed thoroughly. The resulting solid mixture was transferred to a 25 mL double-necked round-bottom flask under an argon atmosphere, to which 15 mL of dry DMF was added. The mixture was sonicated and purged with argon

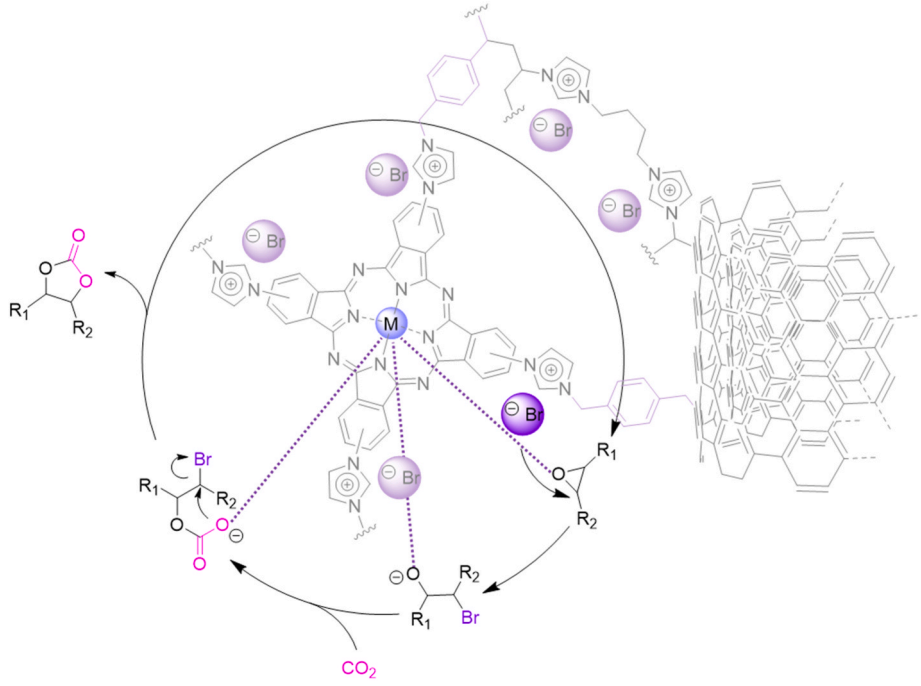

Fig. 5. Mechanism for the synthesis of cyclic carbonates via cycloaddition of CO_2 to epoxides highlighting the synergistic effect between the Lewis acid center and the nucleophile.

Table 1
Conversion of epichlorohydrin into 4-chloromethyl-1,3-dioxolan-2-one catalysed by **MPC@MWCNT**.

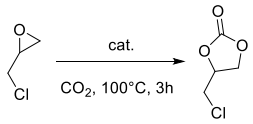

Entry	Catalyst	Metal Loading[a] (μmol)	Conversion	Selectivity	TON	TOF (h^{-1})
1	**MWCNT**	n.a.	traces	n.a.	n.a.	n.a.
2	**MgPC@MWCNT**	38 μmol	41 %	>99 %	3300	1100
3	**CuPC@MWCNT**	42 μmol	27 %	>99 %	1970	660
4	**ZnPC@MWCNT**	35 μmol	12 %	>99 %	1050	350

Reaction conditions: epichlorohydrin (24 mL, 306 mmol), catalyst (160 mg, 0.010–0.014 mol% of metal), CO_2 (25 bar), 100 °C, 3h, 500 r.p.m. Conversion were determined using ^{1}H NMR analysis (Fig. S12–S15). [a)] Referred to 160 mg of catalyst. To have information regarding TON and TOF values calculated with respect to the nucleophile Br^- please consult Table S3.

for 20 min. Afterward, freshly recrystallized AIBN (1 eq) was introduced, and the mixture was stirred at 110 °C overnight. Once cooled down to room temperature, a dark blue colored solid was observed; this solid was filtered, washed twice with hot water, twice with hot methanol, three times with acetone, and finally dried at 60 °C overnight to obtain the desired **MPC@MWCNT**.

MgPC@MWCNT: 670 mg obtained (98 %) from 300 mg (0.19 mmol) of **MgPC-(Imi-Styryl)$_4$Br$_4$**, 285 mg (0.70 mmol) of **Bis-Vinyl-Imi-Br**, and 95 mg of MWCNT.

CuPC@MWCNT: 782 mg obtained (97 %) from 355 mg (0.22 mmol) of **CuPC-(Imi-Styryl)$_4$Br$_4$**, 340 mg (0.84 mmol) of **Bis-Vinyl-Imi-Br**, and 112 mg of MWCNT.

ZnPC@MWCNT: 370 mg (81 %) obtained from 200 mg (0.12 mmol) of **ZnPC-(Imi-Styryl)$_4$Br$_4$**, 190 mg (0.47 mmol) of **Bis-Vinyl-Imi-Br**, and 65 mg of MWCNT.

2.5. Catalytic experiments

Catalytic experiments were carried out using a Cambridge Design Bullfrog batch reactor, which features temperature control and mechanical stirring. This reactor also allows for pressure monitoring, ensuring precise control during the experiments. Prior to each test, the catalyst material was dried overnight in a vacuum oven set at 60 °C to remove any moisture. During each experiment, 20–24 mL of epoxide was introduced into a PTFE vial, where the catalyst was added under solvent-free conditions. After securely closing the reactor, the mixture was stirred at 500 rotations per minute (r.p.m.). To establish an inert atmosphere, the system was purged with nitrogen for 10 min before introducing 25 bar of carbon dioxide (CO_2). Following the gas addition, the reaction mixture was heated to the desired temperature at a rate of 5 °C/min. The temperature was maintained throughout the designated reaction time to ensure optimal conditions. Upon completion of the reaction, the reactor was allowed to cool to room temperature before being depressurized. The catalyst was subsequently separated from the reaction mixture through filtration using a Millipore filter with a pore size of 0.45 μm. The resulting filtrate was then analyzed via ^{1}H NMR in $(CD_3)_2SO$ to assess the composition of the reaction mixture.

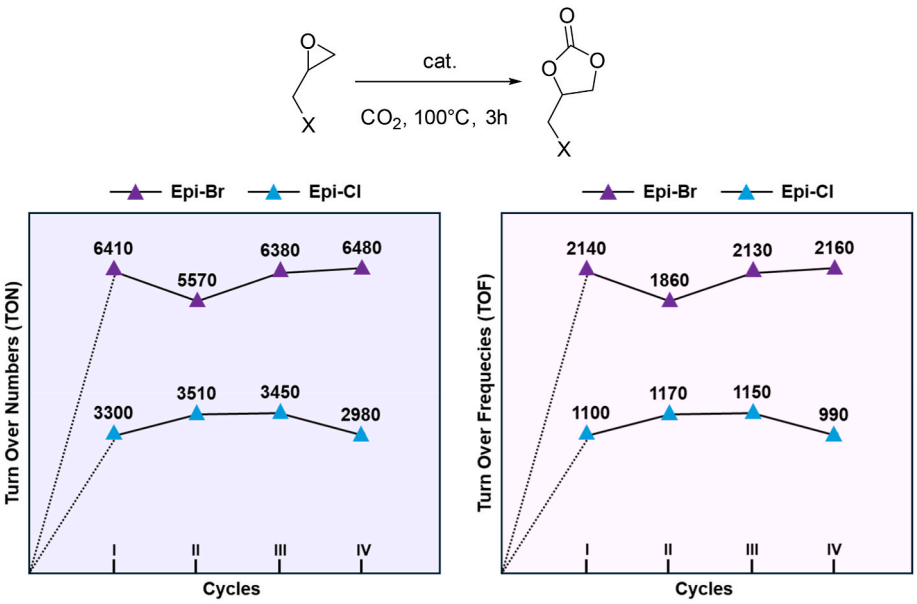

Fig. 6. TON and TOF values calculated basing on the Mg content in **MgPC@MWCNT** used as catalyst for the conversion of both epichlorohydrin and epibromohydrin into their corresponding cyclic carbonates. Initial reaction conditions with epichlorohydrin: 24 mL of epoxide (306 mmol), 160 mg of catalyst (38 μmol of Mg), 25 bar of CO_2, 100°C, 3h. Initial conditions with epibromohydrin: 20 mL of epoxide (233 mmol), 100 mg of catalyst (24 μmol of Mg), 25 bar of CO_2, 100°C, 3h. Conversion values were determined using ^{1}H NMR analysis (Figs. S16–S19 and Fig. S23–S26). The reaction conditions of each cycle are in the Supporting Information in the description of each NMR spectrum. For all catalytic recycling tests the selectivity was >99 %.

2.6. Recycling tests

Recycling tests were conducted to evaluate the cycloaddition reaction between epichlorohydrin and CO_2, and also between epibromohydrin and CO_2. Upon completion of the reaction, the catalytic material was recovered through Millipore filtration using a filter with a pore size of 0.45 μm. To ensure a good cleaning, the catalyst was washed sequentially: three times with 50 mL of toluene, three times with 50 mL of ethanol, and once with diethyl ether. Before the next reaction cycle, the catalyst was dried overnight in a vacuum oven maintained at 60 °C. Once dried, the catalyst was reused in the subsequent cycle, carefully maintaining the same molar ratio between the catalyst weight and the epoxides to ensure consistency in each recycle test.

3. Results and discussion

The three **MPC-Im$_4$** compounds were synthetized using Mg, Cu and Zn, according to the procedure that we already described in our previous work [23] (Fig. 1): 4-nitrophthalonitrile was converted into 4-(1*H*-imidazole-1-yl)phthalonitrile which has been used as building block for the templated synthesis of the various metal phthalocyanines that have been obtained as a mixture of four statistical regio-isomers.

Following their characterization (Table S1, Figs. S1–S2), the three **MPC-Im$_4$** have been functionalized by quaternizing their imidazole moieties with 4-benzylvinyl bromide, resulting in three different intermediates **MPC-(Imi-Styryl)$_4$Br$_4$** (Fig. 1). Comparing the UV spectra of these intermediates with those of their precursors **MPC-Im$_4$** (Fig. S1), no significant differences are observed. This confirms that the quaternization process of the imidazoles did not significantly alter the electronic properties of the three different phthalocyanine cores. In both sets of spectra, the Soret band (B band, 300–400 nm) can be distinguished, which is associated with π–π* electronic transitions between the molecular orbitals of the conjugated phthalocyanine system [37]. Additionally, the Q band (600–750 nm), characteristic of metallated phthalocyanines, is also present [37]. This band is responsible for absorption in the visible and near-infrared regions and is often split into two peaks for asymmetric phthalocyanines. In both sets of spectra, small shoulders of the Q bands can be observed in the 600–650 nm region. These signals arise when the electronic symmetry of the phthalocyanine is disturbed due to the polar nature of the solvent and the tendency of these substrates to aggregate at the molecular level [37]. The quaternization of the four imidazole rings into imidazolium bromide moieties was confirmed and quantified by means of Fourier transform-infrared (FT-IR) spectroscopy and X-ray photoelectron spectroscopy (XPS) measurements, respectively. From the FT-IR spectra acquired for each **MPC-(Imi-Styryl)$_4$Br$_4$** (Fig. S2), it is possible to observe a significant increase in a band between 2700 and 3100 cm^{-1}, corresponding to the stretching of C–H bonds from both aromatic and aliphatic carbon atoms present in the newly introduced styryl groups. The stretching vibration bands of the C=C and C=N bonds present in the aromatic core of the phthalocyanine are located between 1495 and 1620 cm^{-1} and overlap with the bands corresponding to the stretching vibration of the vinyl C=CH$_2$ double bond present in the various **MPC-(Imi-Styryl)$_4$Br$_4$**. The new large band located around 3400 cm^{-1} corresponds to the presence of O–H bonds from water molecules adsorbed by the notoriously hygroscopic imidazolium bromide fractions. The XPS survey spectra of the three **MPC-(Imi-Styryl)$_4$Br$_4$** compounds (Fig. S3) confirm the presence of Br$^-$. A closer examination of the high-resolution XPS spectra in the Br3d region (Fig. S3) reveals an intense signal that has been deconvoluted into two distinct peaks referring to the Br3d$_{3/2}$ and Br3d$_{5/2}$ typical peaks. Similarly, the high-resolution XPS spectra of the N1s region for all three **MPC-(Imi-Styryl)$_4$Br$_4$** compounds (Fig. S3) exhibit two well-defined signals: the first one appears at 398 eV and corresponds to the nitrogen atoms within the phthalocyanine core while second signal, appearing at c.a. 402 eV is associated with nitrogen atoms present in the imidazole rings. The area under the curve (A.U.C.) values associated with these signals possess the expected ratio of *circa* 1:1; therefore, it was possible to confirm that, for all the three **MPC-Im$_4$**, most imidazole rings were successfully quaternized and converted into imidazolium bromide fractions. Once characterized, the various **MPC-(Imi-Styryl)$_4$Br$_4$** have been co-polymerized together with **Bis-Vinyl-Imi-Br** in the presence of MWCNT to produce the three **MPC@MWCNT** materials (Fig. 1) *via* a random radical polymerization process [18–23]. In this regard, it is important to emphasize that the synthesis process shown in Fig. 1 represents a simple yet highly effective method for the covalent functionalization of substantial amounts of metal-phthalocyanine onto

MWCNT. The versatility of this approach lies primarily in the possibility to choose the metal center in the starting phthalocyanine, and the linker as well. This aspect allows to strategically design materials displaying specific functions: indeed, this "lego-like" approach offers the potential to create a wide variety of materials, each with a potential use in several fields of Materials Science.

The FT-IR spectra acquired for the three **MPC@MWCNT** (Fig. S4) exhibit the same types of bands previously observed for their precursors thus confirming the presence of both imidazolium and phthalocyanine moieties: specifically, despite the samples have been dried at 60 °C for 3h before the analysis, the bands at 3400 cm^{-1} corresponding to the vibrational stretching of O–H bonds from water molecules is still visible as a consequence of the adsorbed H_2O onto the very hygroscopic imidazolium fractions**;** the bands between 2700 and 3100 cm^{-1} correspond to the stretching of C–H bonds, and finally, the bands between 1450 and 1620 cm^{-1} are due to the vibrational stretching of C═C and C═N bonds present in the aromatic core of the phthalocyanines. Lastly, there are also some bands in the range of 1000 and 1200 cm^{-1} which are consistent with the bending vibration modes of both aliphatic and aromatic C–H bonds (Fig. S4). The morphology of these materials was investigated using Transmission Electron Microscopy (TEM): TEM micrographs obtained for all three **MPC@MWCNT** solids (Fig. 2) show clearly that in all the cases the co-polymerization process occurred uniformly across the surface of the MWCNT, so to have the **MPC-(Imi-Styryl)$_4$Br$_4$/Bis-Vinyl-Imi-Br** co-polymer following the scaffold of the nanotubes. In combination with this outcome, EDX micrographs (Fig. S5–S7) of the three materials show that there is not segregation of phase, thus suggesting an uniform distribution of their elemental components (and therefore of their active sites) all over the shape of the nanotubes.The specific surface area (SSA) of each **MPC@MWCNT** has been calculated exploiting the Brauner- Emmett- Teller (BET) equation [38], and resulted in 80 m^2/g, 100 m^2/g and 80 m^2/g for **MgPC@MWCNT**, **CuPC@MWCNT** and **ZnPC@MWCNT**, respectively. The three materials supported onto MWCNT show a higher SSA than the one related to the analogous unsupported material **MgPC–SIBI–Br** (40 m^2/g) [23]. This result can be ascribed to the presence of the MWCNT (SSA of 240 m^2/g) which served as an effective templating scaffold for the co-polymerization process. Their large specific surface area provided an extensive interface for co-polymer growth, favouring the integration of the co-polymer onto the nanostructure.

Solid-state cross-polarization magic angle spinning ^{13}C nuclear magnetic resonance (ss CP-TOSS-MAS ^{13}C NMR) spectroscopy performed employing total suppression spinning sidebands (TOSS) pulse sequence on the three **MPC@MWCNT** samples (Fig. 3) reveals the presence of aromatic carbon signals in all of them. These signals arise from the resonance of carbon atoms within the phthalocyanine, imidazolium, and phenyl ring structures, and are grouped in the 120–155 ppm region. Additionally, signals in the region between 25 and 60 ppm correspond to contributions from various aliphatic carbon atoms present in the materials.

It is noteworthy that, in the case of **CuPC@MWCNT**, the signal at approximately 150 ppm, which is observed for both **MgPC@MWCNT** and **ZnPC@MWCNT**, is absent. This signal is likely associated with the carbon atoms in the core of the phthalocyanine ring, specifically those closest to the metal center of the phthalocyanine complex. Since Cu(II) is a paramagnetic species, it is possible that this signal has been shifted or even suppressed due to the paramagnetic nature of the metal itself [39]. This phenomenon does not occur with **MgPC@MWCNT** and **ZnPC@MWCNT**, as Mg(II) and Zn(II) are diamagnetic species. This hypothesis finds another confirmation in the ss CP-TOSS-MAS ^{13}C NMR spectra acquired for the three **MPC-Im$_4$** (Fig. S8): besides the worse signal-to-noise ratio in the copper phthalocyanine spectrum, the signal trend of the three phthalocyanines match the trend of contribution observed in the NMR spectra of their respective materials concerning the signal at 150 ppm *ca.*

Thermogravimetric analysis (TGA) was conducted under both air and nitrogen flow for the three **MPC@MWCNT** (Fig. 4). As expected, the three hybrids exhibit different degradation profiles depending on the type of gas flow used during the analysis. However, apart from slight variations in percentage weight loss, **MgPC@MWCNT**, **CuPC@MWCNT** and **ZnPC@MWCNT** display similar degradation profiles when compared within the same TGA analysis under identical gas flow conditions (air or N_2). This observation aligns with the type of synthesis used to prepare these materials: indeed, during the aforementioned polymerization process, it is possible for the final material to incorporate a larger amount of **Bis-Vinyl-Imi-Br** compared to **MPC-(Imi-Styryl)$_4$Br$_4$**, or *vice versa*. This could lead to slight variations in the overall composition of the materials, without significantly affecting their general properties though. In this regard, all the three **MPC@MWCNT** demonstrate remarkable resistance to thermal stress, showing the first degradation peaks above 300 °C in both air and N_2 flow. Notably, in TGAs conducted under air flow, the curves for all three **MPC@MWCNT** samples do not reach zero; instead, a residual mass (<5 %) persists, corresponding to metal oxides formed during the analysis.

XPS analyses of the three **MPC@MWCNT** materials confirmed the presence of all expected elements, as shown in their survey spectra (Fig. S10; see Fig. S11 for the XPS dataset of pristine MWCNT). Also in this case, the high-resolution XPS spectra for the N1s region (Fig. S10) reveal two distinct nitrogen contributions, corresponding to the different nitrogen types in these materials. For **MgPC@MWCNT**, **CuPC@MWCNT**, and **ZnPC@MWCNT**, the nitrogen signal related to phthalocyanine moieties (PC–N) consist in a peak at 398.5 eV, with A.U.C. values of 26 %, 25 %, and 23 %, respectively. Meanwhile, the nitrogen signal associated with imidazolium moieties (Imi-N) is located at 401.5 eV, with A.U.C. values of 74 %, 75 %, and 77 %, respectively (Fig. S10). These XPS results have been combined with the ones of elemental analysis in order to calculate the metal loading of each material (Table S2), which resulted equal to 0.24 mmol/g for **MgPC@MWCNT**, 0.26 mmol/g for **CuPC@MWCNT** and 0.22 mmol/g for **ZnPC@MWCNT**.

Hence, after complete characterization, the three **MPC@MWCNT** have been tested as catalyst for the conversion of epichlorohydrin into the corresponding cyclic carbonate in the presence of CO_2. In our previous works [19,23, see Table S3], we have already emphasized how the cycloaddition of CO_2 and epoxides in cyclic carbonates is a process significantly enhanced by the synergistic action of a Lewis acid and a nucleophile that operate with a certain proximity to each other (Fig. 5): the epoxide interacts with the metal cation, enhancing its reactivity toward nucleophilic attack by the bromide ion. This interaction forms an initial intermediate, which then undergoes a reaction with CO_2, producing a second intermediate. The subsequent closure of this intermediate results in the formation of the cyclic carbonate and the liberation of the bromide ion.

Considering that this reaction, under the same conditions, do not occur without a catalyst [18] and neither employing only MWCNT (Table 1 entry 1), it is possible to state that all three materials are catalytically active for the title reaction. They all demonstrate excellent levels of selectivity (Table 1 entries 2–4); however, **MgPC@MWCNT** appears to be the most active catalyst among the three, as demonstrated by TON (defined as the moles of product obtained per mole of active sites - Mg, Cu, Zn and Br^-) and TOF (TON divided by reaction time in hours) values. Given that the primary difference among the three materials lies in the metal cation coordinated to the phthalocyanine, the catalytic efficiency trend observed in Table 1 (**MgPc@MWCNT** > **CuPc@MWCNT** > **ZnPc@MWCNT**) is most likely governed by the nature of the metal ions. The Lewis acidity of the metal center plays a key role in promoting the cycloaddition of CO_2 with epoxides to form cyclic carbonates. Accordingly, the observed catalytic order can be rationalized by the relative Lewis acid hardness of the metal cations, which follows the trend $Mg^{2+} > Cu^{2+} > Zn^{2+}$ [40].

The recyclability of the best catalyst of the serie (**MgPC@MWCNT)** under the same operating conditions was evaluated. TONs and TOFs

related to the conversion of epichlorohydrin, are presented in Fig. 6.

These data indicate that the material can be successfully recycled, showing an increased activity after the first cycle and a slight reduction of the catalytic activity in the fourth cycle. To understand the reasons of the slight decrease in the catalytic performances at the fourth cycle, an XPS analysis was conducted on **MgPC@MWCNT** after reuse. This analysis revealed that the material no longer contained bromine but instead chlorine. Notably, further investigation, once again conducted *via* XPS (Fig. S20–S22), displayed that anion substitution took place after the first catalytic cycle not only for **MgPC@MWCNT**, but also for **CuPC@MWCNT** and **ZnPC@MWCNT** (Table 1). This observation led us to hypothesize that the bromide anions from the imidazole fractions likely exchanged with the chlorine atoms from the epoxy reagent or, possibly, with any chlorinated intermediates or products present in the reaction mixture. Regardless of the source substrate for the exchange, although the occurrence of this bromine-to-chlorine nucleophilic substitution seemed not impair the recyclability of **MgPC@MWCNT**, it probably led to an underestimation of its actual catalytic activity. To shed light on this catalytic behavior, additional tests were performed employing epibromohydrin. This epoxide substrate is similar to epichlorohydrin, but it is unable to give the bromine-chlorine exchange mentioned above. Interestingly, the TONs and TOFs values were higher than those obtained with epichlorohydrin (Fig. 6) thus confirming the previous hypothesis and highlighting even more the excellent catalytic performances of **MgPC@MWCNT**. Moreover, also in the case of this epoxydic substrate, **MgPC@MWCNT** proved to be recyclable up to four cycles without any decrease of the catalytic performances (Fig. 6). XPS spectroscopy and CHN elemental analysis were carried out on **MgPC@MWCNT** after the fourth catalytic cycle with epibromohydrin (Table S2, Fig. S27). The high-resolution XPS spectrum of the Br 3d region (Fig. S27) confirms the presence of bromine in two distinct chemical states: as a bromide anion (Br $3d_{3/2}$ at 68.4 eV and Br $3d_{5/2}$ at 67.3 eV) and as an alkyl bromide (Br $3d_{3/2}$ at 71.2 eV and Br $3d_{5/2}$ at 70.1 eV) [41]. The alkyl bromide signal likely originates from residual brominated reagents or products adsorbed on the **MgPC@MWCNT** surface, despite washings after the final cycle. The N 1s high-resolution spectrum (Fig. S27) reveals contributions from Imi-N and PC-N of 76 % and 24 % A.U.C., respectively. These values closely match those of fresh **MgPC@MWCNT** prior to catalytic use. When these XPS findings are combined with CHN elemental analysis (Table S2), the metal loading after four cycles is estimated to be 0.21 $mmol_{Mg}/g$, which is very close to the initial value of 0.24 mmol/g estimated for the fresh material. This result highlights the robustness of the catalyst and indicates minimal Mg leaching during recycling.

Furthermore, after confirming its recyclability, **MgPC@MWCNT** was also evaluated for its ability to convert other epoxydic substrates under different reaction conditions, achieving notable results (Table 2).

MgPC@MWCNT has demonstrated remarkable versatility in promoting the conversion of different epoxides into the corresponding cyclic carbonates. Moreover, the different temperatures and reaction times to which this material has been subjected allows highlighting its extraordinary resistance to both thermal and mechanical stress. The high TON achieved in the case of glycidol (entry 1) evidences the efficiency of the catalyst when moderate temperatures and relatively long

Table 2
Conversion of different epoxides into their corresponding cyclic carbonate catalysed by **MgPC@MWCNT**.

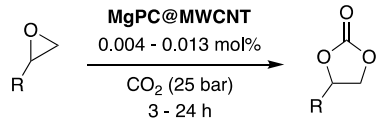

Entry	substrate	Temperature(°C)	time (h)	Conversion (%)	Selectivity (%)[a]	TON	TOF (h-1)[b]
1[c]	360 mmol	80	24	75	>99	19290	805
2[d]	306 mmol	100	8	73	>99	5880	755
3[e]	255 mmol	100	3	44	>99	3510	1170
4[f]	280 mmol	100	3	82	>99	6040	2010
5[g]	233 mmol	100	3	64	>99	6480	2160
6[h]	210 mmol	125	24	69	>99	10350	450
7[i]	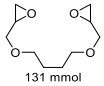 131 mmol	125	24	46	>99	8610	360

[a] Selectivity towards the corresponding cyclic carbonate.
[b] Values calculated towards the amount of Mg in the catalyst, to see TON and TOF values towards the nucleophile Br^- see Table S4.
[c] 24 mL of epoxide (360 mmol), 60 mg cat. (14 μmol of Mg), CO_2 25 bar + refill after 8h.
[d] 24 mL of epoxide (306 mmol),160 mg cat. (38 μmol of Mg), CO_2 25 bar.
[e] 20 mL of epoxide (255 mmol), 134 mg cat. (32 μmol of Mg), CO_2 25 bar, this entry corresponds to the 2nd cycle with epichlorohydrin operated by **MgPC@MWCNT**;
[f] 24 mL of epoxide (280 mmol),160 mg cat. (38 μmol of Mg), CO_2 25 bar.
[g] 20 mL of epoxide (233 mmol), 95 mg cat. (23 μmol of Mg), CO_2 25 bar, this entry corresponds to the 4th cycle with epibromohydrin operated by **MgPC@MWCNT**;
[h] 24 mL of epoxide (210 mmol), 60 mg cat. (14 μmol of Mg), CO_2 25 bar.
[i] 24 mL of epoxide (131 mmol), 60 mg cat. (14 μmol of Mg), CO_2 25 bar; Conversion values have been estimated via ^{1}H NMR (Fig. S28–S34).

reaction times are employed. In the case of epichlorohydrin, it is possible to observe that, under the same conditions, a longer reaction time led to higher conversion levels (entries 2 and 3). Concerning the more reactive epibromohydrin, it can be observed that, with other conditions being equal, using a larger amount of catalyst results in higher conversion levels more quickly compared to using a smaller amount of catalyst (see entries 4 and 5). Finally, entries 6 and 7 show that, despite using small amounts of catalyst to convert different types of epoxy-substrates, increasing both the time and temperature conditions allows for significant conversions, which could certainly be increased by employing larger quantities of catalyst. It is noteworthy that all the above reactions have been carried out using extremely low Lewis acid catalytic loading ranging from 0.004 mol% (entry 1) to 0.013 mol% (entry 4).

Comparing the catalytic results achieved by **MgPC@MWCNT** with those of similar systems already reported in the literature (including our own, see Table S5 for comparison), it can be stated that this material is one of the most active fully heterogeneous catalyst based on metal-phthalocyanines and imidazolium bromide in promoting the cycloaddition of epoxides and CO_2 into cyclic carbonates. Considering that no studies have yet described **MWCNT**-supported bifunctional heterogeneous materials based on imidazolium bromide and metal-phthalocyanines applied for the thermo-induced conversion of CO_2 into cyclic carbonates in the presence of epoxides, these catalytic results are even more valuable. To know the values of TON and TOF calculated with respect to the nucleophile Br^- of all the materials discussed until know, please refer to Table S3 and Table S4.

4. Conclusions

In the present study, three different MWCNT-supported bifunctional heterogeneous materials based on imidazolium bromide and various metal-phthalocyanines were prepared. After thorough characterization using techniques such as solid-state NMR spectroscopy, XPS, TEM, EDX, FT-IR, CHN, N_2 physisorption, and TGA, these materials were tested for their ability to catalyse the conversion of epoxides to cyclic carbonates in the presence of CO_2. The main goal was to identify any differences in catalytic activity between these MWCNT-supported materials and their unsupported counterparts already reported in the literature by us [23]. Based on the catalytic tests performed, it can be concluded that, under the same conditions, the **MgPC@MWCNT** material outperforms its unsupported analogue, **MgPC–SIBI–Br** (Table S3). This is likely due to the presence of MWCNT, which provides **MgPC@MWCNT** with a larger surface area compared to **MgPC-BIBI-Br**, where the nanotubes are absent. Most likely, this results in greater exposure of the active sites in the MWCNT-supported materials. In addition to these new findings, it is worth to remark again that the current study introduces a simple yet highly effective approach for covalently attaching large amounts of metal-phthalocyanine onto MWCNT. This is a crucial aspect, not only because, to the best of our knowledge, modern literature lacks approaches that can yield similar results, but also because this "lego-like" strategy has the potential to create a diverse range of materials, each build with a different metal-phthalocyanine, and therefore useable in many different catalytic contexts.

CRediT authorship contribution statement

Benedetto Taormina: Writing – original draft, Visualization, Validation, Investigation, Formal analysis, Data curation. **Rémy Jouclas:** Investigation, Data curation. **Alwyn Dsouza:** Investigation, Data curation. **Anthony Morena:** Writing – review & editing, Investigation, Data curation. **Michelangelo Gruttadauria:** Writing – review & editing, Validation, Supervision. **Carmela Aprile:** Writing – review & editing, Validation, Supervision, Resources, Project administration, Methodology, Funding acquisition, Conceptualization. **Francesco Giacalone:** Writing – review & editing, Validation, Supervision, Project administration, Methodology, Funding acquisition, Conceptualization.

Declaration of competing interest

The authors declare that they have no known competing financial interests or personal relationships that could have appeared to influence the work reported in this paper.

Acknowledgement

This research was funded by University of Palermo and the Italian Ministry of Education (PRIN 2017 project no. 2017W8KNZW). This research is supported by the F.R.S-FNRS via funding grants GEQ U. G014.19 EQP U.N034.17 and PDR T.0004.21, European Regional Development Fund (FEDER) and the Walloon Region (Low Carbon Footprint Materials – BIORG-EL project. B. T. gratefully acknowledges the University of Palermo and University of Namur for a co-funded PhD fellowship. The authors acknowledge Dr. Luca Fusaro and Dr. Alberto Spinella for their support to the NMR experiments. This research used resources of PC2 (Plateforme Technologique Physico-Chemical Characterization), MORPH-IM (Morphology & Imaging) and SIAM (Synthesis, Irradiation & Analysis of Materials) technology platforms located at the University of Namur.

Appendix A. Supplementary data

Supplementary data to this article can be found online at https://doi.org/10.1016/j.carbon.2025.120508.

References

[1] J. Sawyer, Man-made carbon dioxide and the “greenhouse” effect, Nature 239 (1972) 23–26, https://doi.org/10.1038/239023a0.
[2] A.G. Olabi, M.A. Abdelkareem, Renewable energy and climate change, Renew. Sustain. Energy Rev. 158 (2022), https://doi.org/10.1016/j.rser.2022.112111, 1364-0321.
[3] P.T. Anastas, J.C. Warner, Green Chemistry: Theory and Practice, Oxford University Press, New York, 1998, p. 30.
[4] E. Alper, CO2 utilization: developments in conversion processes, Petroleum 3 (2017) 2405–6561, https://doi.org/10.1016/j.petlm.2016.11.003.
[5] M. Aresta, A. Di Benedetto, A. Angelini, Catalysis for the valorization of exhaust carbon: from CO2 to chemicals, materials, and fuels. Technological use of CO2, Chem. Rev. 114 (2014) 1709–1742, https://doi.org/10.1021/cr4002758.
[6] M. North, R. Pasquale, C. Young, Synthesis of cyclic carbonates from epoxides and CO2, Green Chem. 12 (2010) 1514–1539, https://doi.org/10.1039/C0GC00065E.
[7] R.R. Shaikh, S. Pornpraprom, V. D’Elia, Catalytic strategies for the cycloaddition of pure, diluted, and waste CO2 to epoxides under ambient conditions, ACS Catal. 8 (2018) 419–450, https://doi.org/10.1021/acscatal.7b03580.
[8] W. Clegg, R.W. Harrington, M. North, F. Pizzato, P. Villuendas, Cyclic carbonates as sustainable solvents for proline-catalysed aldol reactions, Tetrahedron Asymmetry 21 (2010) 1262–1271, https://doi.org/10.1016/j.tetasy.2010.03.051.
[9] J.H. Clements, Reactive applications of cyclic alkylene carbonates, Ind. Eng. Chem. Res. 42 (2003) 663–674, https://doi.org/10.1021/ie020678i.
[10] B. Schäffner, F. Schäffner, S.P. Verevkin, A. Börner, Organic carbonates as solvents in synthesis and catalysis, Chem. Rev. 110 (2010) 4554–4581, https://doi.org/10.1021/cr900393d.
[11] N. Podrojková, V. Sans, A. Oriňak, R. Oriňaková, Recent developments in the modelling of heterogeneous catalysts for CO2 conversion to chemicals, ChemCatChem 12 (2020) 1802, https://doi.org/10.1002/cctc.201901879.
[12] H.S. Whang, J. Lim, M.S. Choi, J. Lee, H. Lee, Heterogeneous catalysts for catalytic CO2 conversion into value-added chemicals, BMC Chem. Eng. 9 (2019), https://doi.org/10.1186/s42480-019-0007-7.
[13] S. Singh Dhankhar, B. Ugale, C.M. Nagaraja, Co-catalyst-free chemical fixation of CO2 into cyclic carbonates by using metal-organic frameworks as efficient heterogeneous catalysts, Chem. Asian J. 15 (2020) 2403–2427, https://doi.org/10.1002/asia.202000424.
[14] P.T.K. Nguyen, H.T.D. Nguyen, H.N. Nguyen, C.A. Trickett, Q.T. Ton, E. Gutiérrez-Puebla, et al., New metal–organic frameworks for chemical fixation of CO2, ACS Appl. Mater. Interfaces 10 (2018) 733–744, https://doi.org/10.1021/acsami.7b16163.
[15] Q.N. Zhao, Q.W. Song, P. Liu, Q.X. Zhang, J.H. Gao, K. Zhang, Catalytic conversion of CO2 to cyclic carbonates through multifunctional zinc-modified ZSM-5 zeolite, Chin. J. Chem. 36 (2018) 187–193, https://doi.org/10.1002/cjoc.201700573.
[16] R. Babu, S.H. Kim, J.F. Kurisingal, H.J. Kim, G.G. Choi, D.W. Park, A room temperature synthesizable zeolitic imidazolium framework catalyst for the solvent-free synthesis of cyclic carbonates, J. CO2 Util. 25 (2018) 6–13, https://doi.org/10.1016/j.jcou.2018.03.006.
[17] A. Morena, V. Campisciano, A. Comès, L.F. Liotta, M. Gruttadauria, C. Aprile, et al., A study on the stability of carbon nanoforms-polyimidazolium network hybrids in

the conversion of CO_2 into cyclic carbonates: increase in catalytic activity after reuse, Nanomaterials (Basel) 11 (9) (2021) 2243, https://doi.org/10.3390/nano11092243.
[18] V. Campisciano, L. Valentino, A. Morena, A. Santiago-Portillo, N. Saladino, M. Gruttadauria, et al., Carbon nanotube supported aluminum porphyrin-imidazolium bromide crosslinked copolymer: a synergistic bifunctional catalyst for CO2 conversion, J. CO2 Util. 57 (2022) 2212–9820, https://doi.org/10.1016/j.jcou.2022.101884.
[19] L. Valentino, V. Campisciano, C. Célis, V. Lemaur, R. Lazzaroni, M. Gruttadauria, et al., Highly cross-linked bifunctional magnesium porphyrin-imidazolium bromide polymer: unveiling the key role of co-catalysts proximity for CO2 conversion into cyclic carbonates, J. Catal. 428 (2023) 21–9517, https://doi.org/10.1016/j.jcat.2023.115143.
[20] P. Gao, S. Li, X. Bu, S. Dang, Z. Liu, H. Wang, et al., Direct conversion of CO2 into liquid fuels with high selectivity over a bifunctional catalyst, Nature Chem 9 (2017) 1019–1024, https://doi.org/10.1038/nchem.2794.
[21] Z.Q. Li, Y.Y. Zhang, Y.J. Zheng, B. Li, G.P. Wu, J. Org. Chem. 87 (2022) 3145–3155, https://doi.org/10.1021/acs.joc.1c02888.
[22] A. Morena, V. Campisciano, A. Santiago-Portillo, M. Gruttadauria, F. Giacalone, C. Aprile, POSS-Al-porphyrin-imidazolium cross-linked network as catalytic bifunctional platform for the conversion of CO2 with epoxides, Fuel (Guildf.) 336 (2023) 16–2361, https://doi.org/10.1016/j.fuel.2022.126819.
[23] B. Taormina, R. Jouclas, V. Marsala, M. Gruttadauria, F. Giacalone, C. Aprile, Imidazolium bromide substituted magnesium phthalocyanine polymers: new promising materials for CO2 conversion, J. CO2 Util. 85 (2024) 2212–9820, https://doi.org/10.1016/j.jcou.2024.102875.
[24] A. Krueger, Carbon Materials and Nanotechnology, Wiley-VCH, Weinheim, 2010, pp. 123–381.
[25] C. Binns, Introduction to Nanoscience and Nanotechnology, John Wiley & Sons, Inc., New Jersey (USA), 2010, pp. 53–95.
[26] K. Tanaka, S. Iijima, Carbon Nanotubes and Graphene, second ed., Elsevier, Amsterdam, 2014.
[27] V. Campisciano, R. Burger, C. Calabrese, L.F. Liotta, P. Lo Meo, M. Gruttadauria, et al., Straightforward preparation of highly loaded MWCNT–polyamine hybrids and their application in catalysis, Nanoscale Adv. 2 (2020) 4199–4211, https://doi.org/10.1039/D0NA00458E.
[28] V. Campisciano, C. Calabrese, L.F. Liotta, V. La Parola, A. Spinella, C. Aprile, et al., Templating effect of carbon nanoforms on highly cross-linked imidazolium network: catalytic activity of the resulting hybrids with Pd nanoparticles, Appl. Organomet. Chem. 33 (2019), https://doi.org/10.1002/aoc.4848, 1099-0739.
[29] V. Campisciano, M. Gruttadauria, F. Giacalone, Modified nanocarbons for catalysis, ChemCatChem 11 (2019) 90–133, https://doi.org/10.1002/cctc.201800976.
[30] L. Valentino, R. Di Forti, A. Morena, C. Aprile, M. Gruttadauria, F. Giacalone, et al., Polymerizable deep eutectic solvents: convenient reactive dispersion media for the preparation of novel multi-walled carbon nanotubes-based functional materials, J. Chem. Eng. 85 (2024) 1385–8947, https://doi.org/10.1016/j.jcou.2024.102875.
[31] B. Sorokin, Phthalocyanine metal complexes in catalysis, Chem. Rev. 113 (2013) 8152–8191, https://doi.org/10.1021/cr4000072.
[32] A. Shaabani, E. Farhangi, Cobalt(II) phthalocyanine catalyzed aerobic regeneration of carbonyl compounds from the corresponding oximes in 1-butyl-3-methylimidazolium bromide, Appl. Catal A: General 371 (2009) 148–152, https://doi.org/10.1016/j.apcata.2009.09.047.
[33] Z. Yu, C. Liu, Y. Deng, M. Li, F. She, L. Lai, Y. Chen, L. Wei, Interfacial engineering of heterogeneous molecular electrocatalysts using ionic liquids towards efficient hydrogen peroxide production, Chin. J. Catal. 42 (2021) 1238–1246, https://doi.org/10.1016/S1872-2067(21)63946-3.
[34] V.B. Khajone, P.R. Bhagat, Brønsted acid functionalized phthalocyanine on perylene diimide framework knotted with ionic liquid: an efficient photo-catalyst for production of biofuel component octyl levulinate at ambient conditions under visible light irradiation, Fuel (Guildf.) 279 (2020) 118390, https://doi.org/10.1016/j.fuel.2020.118390.
[35] V.B. Khajone, K.R. Balinge, D.S. Patle, P.R. Bhagat, Synthesis and characterization of polymer supported Fe-phthalocyanine entangled with carboxyl functionalized benzimidazolium moiety: a heterogeneous catalyst for efficient visible-light-driven degradation of organic dyes from aqueous solutions, J. Mol. Liq. 288 (2019) 111032, https://doi.org/10.1016/j.molliq.2019.111032.
[36] L. Wang, Z. Feng, Q. Hou, Z. Dang, Y. Yu, C. Yang, B. Tang, Q. Zhou, X. Hua, R. Wei, T.X. Liu, Quaternary ammonium salt functionalized copper phthalocyanine-graphene oxide hybrids for cocatalyst-free carbon dioxide cycloaddition, Adv. Compos. Hybrid Mater. 8 (2025) 40, https://doi.org/10.1007/s42114-024-01081-4.
[37] M. Wang, K. Ishii, Photochemical properties of phthalocyanines with transition metal ions, Coord. Chem. Rev. 468 (2022) 10–8545, https://doi.org/10.1016/j.ccr.2022.214626.
[38] S. Brunauer, P.H. Emmett, E. Teller, Adsorption of gases in multimolecular layers, J. Am. Chem. Soc. 60 (1938) 309–319, https://doi.org/10.1021/ja01269a023.
[39] J. Koppe, A.J. Pell, Structure determination and refinement of paramagnetic materials by solid-state NMR, ACS Phys. Chem. Au 3 (2023) 419–433, https://doi.org/10.1021/acsphyschemau.3c00019.
[40] H. Xu, D.C. Xu, Y. Wang, Natural indices for the chemical hardness/softness of metal cations and ligands, ACS Omega 2 (2017) 4431–4442, https://doi.org/10.1021/acsomega.7b01039.
[41] V.V. Multian, F.E. Kinzerskyi, A.V. Vakaliuk, L.M. Grishchenko, V.E. Diyuk, O. Y. Boldyrieva, V.O. Kozhanov, O.V. Mischanchuk, V.V. Lisnyak, V.Ya Gayvoronsky, Surface response of brominated carbon media on laser and thermal excitation: optical and thermal analysis Study, Nanoscale Res. Lett. 12 (2017) 146, https://doi.org/10.1186/s11671-017-1873-7.